Electronic structure, hyperfine parameters and magnetic properties of RFe11Ti intermetallic compounds (R = Y, Pr): Ab initio calculations, SQUID magnetometry and Mössbauer studies

M. Bouhbou, R. Moubah, E.K. Hlil, H. Lassri, Lotfi Bessais

Version of Record: https://www.sciencedirect.com/science/article/pii/S0304885320323295
Manuscript_13bb727251c61b42c8b2cdac6b4eebe4

Electronic structure, hyperfine parameters and magnetic properties of $RFe_{11}Ti$ intermetallic compounds (R= Y, Pr): Ab initio calculations, SQUID magnetometry and Mössbauer studies

M. Bouhbou,[1] R. Moubah,[1] E. K. Hlil,[2] H. Lassri,[1] and L. Bessais[3]

[1] *LPMMAT, Faculty of Sciences Ain Chock Hassan II University of Casablanca, BP 5366 Maarif, Casablanca, Morocco*

[2] *Institut Néel, CNRS et Université Grenoble Alpes, BP 166, 38042 Grenoble, France*

[3] *Univ. Paris Est Créteil, CNRS, ICMPE, 2 rue Henri Dunant F-94320 Thiais, France*

(Dated: July 8, 2020)

Abstract

$RFe_{11}Ti$ (R =Y, Pr) intermetallic compounds were successfully synthesized by arc-melting method. The correlation between their structural and magnetic properties has been investigated by means of X-ray diffraction analysis (XRD), Mössbauer spectrometry and magnetic measurements. The combination of these methods allowed to determine unambiguously the preferred inequivalent crystallographic site of titanium atoms. $PrFe_{11}Ti$ presents a weighted average hyperfine field higher than $YFe_{11}Ti$ compound. For both compounds, the hyperfine field follows this sequence: $H_{\mathrm{HF}}\{8i\} > H_{\mathrm{HF}}\{8j\} > H_{\mathrm{HF}}\{8f\}$. First principles calculations of $RFe_{11}Ti$ were performed utilizing the density functional theory (DFT) based on the full potential linearized augmented plane wave (FLAPW). These calculated data were found to be in good agreement with the experimental magnetic results.

PACS numbers: 75.50.Bb, 75.50.Tt, 76.80.+y

Keywords: Intermetallic compounds; Magnetic materials; DFT; Electronic structure ; Mössbauer spectrometry.

I. INTRODUCTION

Rare-earth transition-metal ($R-T$) magnetic $4f-3d$ intermetallic compounds have been continuously studied for decades. The two magnetic sublattices present in the same alloy bring a simultaneous complementary behavior of the R strong anisotropy properties associated with those of T high magnetic moment. This makes $R-T$ intermetallics potential candidates for hard magnetic materials, high density recording media and magnetic refrigeration[77–90].

In an effort to reduce the content of rare earth metals in $R-T$ intermetallic compounds, and at the same time use low-cost magnetic materials, interest in 1:12 compounds with a tetragonal type structure $I4/mmm$ $ThMn_{12}$ has been renewed [78, 79, 86–103]. It is worth to notice that from a point of view of permanent magnet applications, it is more interesting to have a high Fe content, since it leads to a decrease in the saturation magnetization and of the Curie temperature [91]. D. B. de Mooij and K. H. J. Buschow have demonstrated [78] that the pure binary RFe_{12} does not exist and it is essential to stabilize this intermetallic compound with a third element M (M = Al, Cr, Mo, Si, Ti, V and W) to form the ternaries

$R\mathrm{Fe}_{12-x}M_x$. The M content x is generally small and it depends on the nature of the M element. Many R-Fe-M ternary phase diagrams have been studied enabling to specify the limit of the solid solution of the ThMn_{12}-type phase and showing the upper and lower limit of x for each different M atoms [104, 105]. The ternary compound $\mathrm{YFe}_{10.8}\mathrm{Ti}_{1.2}$ was studied by D. B. de Mooij and K. H. J. Buschow [78]. Z. Liu *et al.* have proven that this ternary compound does not decompose down to 873 K [105].

For ThMn_{12}-type structure, the iron transition metal atoms occupy three inequivalent crystallographic sites $8i$, $8j$ and $8f$. The $3d$ iron rich ThMn_{12}-type intermetallic compounds are expected to exhibit a high saturation magnetization. In addition, due to the large a/c ratio, strong magnetocrystalline anisotropy is awaited. P. Qian *et al.* [106] have demonstrated that the crystal cohesive energy of $\mathrm{Pr(Fe,Ti)}_{12}$ decrease markedly by adding a ternary element Ti. This result indicates that Ti helps to stabilize the crystal structure. Using pair potentials based on *ab initio* calculations, they have shown that the stabilizing element Ti prefers to substitute for Fe in $8i$ sites [106].

In this paper, we have calculated the electronic structure of $\mathrm{YFe}_{11}\mathrm{Ti}$ and $\mathrm{PrFe}_{11}\mathrm{Ti}$, from the first principles based on density functional theory built on the Full Potential Augmented Plane Wave. The calculated magnetic moments have been compared to the experimental results of magnetic measurements and to the hyperfine fields measured by Mössbauer spectrometry.

II. CALCULATION METHOD

The objective of the calculations is to determine the total energy, the magnetic moments as well as the hyperfine field of the intermetallic compound by finding the right spin densities. For this purpose, the Kohn-Sham equations for a particle in a coherent way [107] will be solved. The calculations are performed using the full potential linearized augmented plane wave (FP-LAPW) method to solve the Kohn-Sham equations [107] of the density functional theory (DFT) [108]. These calculations were conducted using the WIEN2k code [109, 110]. The generalized gradient approximation (GGA) with the full Perdew-Burke-Ernzerhof (PBE) correlation energy was used [111].

The cut-off parameter was chosen as follows $R_{\mathrm{MT}} \times K_{\max} = 7$, with $K_{\max}$, the magnitude of the largest $\vec{K}$ vector. We choose $G_{\max} = 12\,\mathrm{Ry}^{\frac{1}{2}}$ for Fourier expansion of potential in the

interstitial region [112] and 1200 k-points were used in the Brillouin zone. The muffin-tin radius R_{MT} were assumed to be 2.50, 2.50, 2.14, and 2.17 Bohr, for Y, Pr, Fe, and Ti atoms, respectively. We have chosen the cut-off energy $E = -7\,\mathrm{Ry}$ in oder to separate the valence and core states. The convergence of self-consistent-field cycle was assumed to be reached and the system was stable when the total energy difference was smaller than $10^{-4}\,\mathrm{Ry}$ and the charge was less than 10^{-4} electron charges.

Another main objective for these calculations is to determine the hyperfine fields for R-Fe-Ti systems, using the same WIEN2 program. This will be done using the self-consistent approach of Blügel *et al.* [113] including relativistic generalizations of the contact, orbital, and dipolar contributions to the hyperfine fields.

III. EXPERIMENTAL

Polycrystalline $R\mathrm{Fe}_{11}\mathrm{Ti}$ (R= Y, Pr) with nominal composition, were prepared by arc-melting technique from high purity elements Y 99.98%, Pr 99.98%, Fe 99.99%, Ti 99.99%. In order to ensure homogeneity, the samples were melted several times [114]. The as-cast ingots were wrapped in tantalum foil and sealed in silica tubes under a vacuum of 10^{-6} mbar, then annealed at 1100°C for 1 week and finally water quenched [115, 116].

The X-ray-diffraction (XRD) with Cu Kα radiation $\lambda = 1.54178\,\text{Å}$ has been recorded on a Bruker D8 diffractometer. The data were collected with a step size of 0.015° and counting time of 13 s from $2\theta = 25°$ to $2\theta = 85°$. The XRD patterns were refined using the FULLPROF program [117, 118] based on the Rietveld method analysis [119, 120]. The shape function was chosen as Thompson-Cox-Hastings pseudo-Voigt type [84, 100, 121, 122]. Two agreement factors (R_B and χ^2) from the program output were used as goodness-of-refinement's indicators.

The Curie temperature (T_C) was measured on a DSM-8 MANICS differential sample Magneto-Susceptometer in a field of 0.1 T. The magnetization curves (M - H) were measured at T = 4.2 K using (PPMS9) Quantum Design under a maximum applied field of 9 T. The M_S values were obtained using the law of approach to saturation.

Mössbauer spectra were collected using Wissel constant-acceleration spectrometer with a 25 mCi Rh matrix Co-57 source [123]. The spectra were analyzed by least-squares fits according to the procedure discussed below. α-Fe standard was used in order to calibrate

the spectrometer. Mössbauer absorbers of $10\,\mathrm{mg/cm^2}$ were prepared from powder samples of $R\mathrm{Fe}_{11}\mathrm{Ti}$. The estimated errors are ± 0.1 T for hyperfine fields $\mu_0 H_{\mathrm{HF}}$ and ± 0.01 mm/s for isomer shifts δ and quadrupole shifts 2ε.

IV. RESULTS AND DISCUSSION

A. Structure analysis

Let's remind that the hexagonal $P6/mmm$ $\mathrm{CaCu_5}$-type structure RT_5 phase is characterized by three Wyckoff positions. R atoms occupy $1a$ $(0,0,0)$ site, whereas T atoms are located in $2c$ $(\frac{1}{3},\frac{2}{3},0)$ and $3g$ $(\frac{1}{2},0,\frac{1}{2})$ crystallographic sites (Figure 1). The relationship between the tetragonal RT_{12} and the hexagonal RT_5 structures can be expressed by the following: the $8i$ site is constituted by $\frac{1}{2}$ atoms of $2c$ site, the $8j$ site comes from $\frac{1}{3}$ of atoms on $3g$ and the remaining $\frac{1}{2}$ of the $2c$ site, whereas, the $8f$ site comes from the other atoms of $3g$ site [124–126]. The $\mathrm{ThMn_{12}}$-type structure occurs when a pair of Fe atoms (dumbbell) replace one R rare-earth atom for the hexagonal $P6/mmm$ $\mathrm{CaCu_5}$-type structure [124–126]:

$$2(RT_5) - R + 2T(\text{dumbbell}) \longrightarrow RT_{12}$$

The following equations show the relationship between the lattice parameters of the the tetragonal $I4/mmm$ $\mathrm{ThMn_{12}}$-type structure and the hexagonal $P6/mmm$ $\mathrm{CaCu_5}$-type structure (Figure 1):

$$a\{\mathrm{CaCu_5}\} = c\{\mathrm{ThMn_{12}}\} \;\text{ and }\; c\{\mathrm{CaCu_5}\} = \frac{1}{2}\, a\{\mathrm{ThMn_{12}}\}$$

Table I. Wyckoff positions and number of atoms in the RT_{12} with $I4/mmm$ tetragonal structure.

	Atomic position	Number of atoms
R $(2a)$	0,0,0	2
T_1 $(8i)$	x,0,0	8
T_2 $(8j)$	x,$\frac{1}{2}$,0	8
T_3 $(8f)$	$\frac{1}{4}$, $\frac{1}{4}$, $\frac{1}{4}$	8

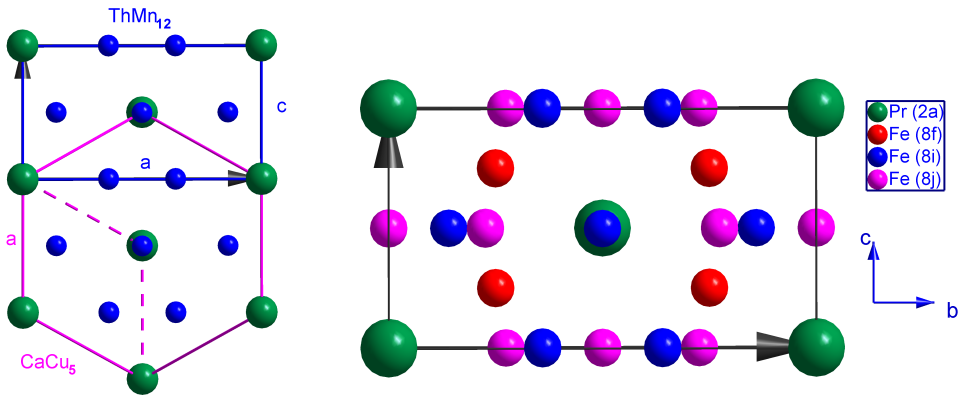

Figure 1. Relationship between $CaCu_5$ and $ThMn_{12}$ structures (left) and crystal structure of the tetragonal $PrFe_{11}Ti$ ($ThMn_{12}$-type structure) with $I4/mmm$ space group (right)

RFe$_{11}$Ti compounds crystallize in the body-centered-tetragonal $ThMn_{12}$-type structure with $I4/mmm$ space group (no. 139), which have $Z = 2$ formula units per unit cell. The three inequivalent crystallographic sites $8i(m2m)$, $8j(m2m)$ and $8f(2/m)$ are occupied by twenty-two $3d$ iron atoms and two $3d$ titanium atoms (Fig. 1 and Table I), while the R atoms occupy the $2a$ site.

The Rietveld refinements of $YFe_{11}Ti$ and $PrFe_{11}Ti$ compounds were performed. Observed, calculated and differential XRD patterns are shown in Figure 2. Positions for the Bragg reflections are marked by vertical bars and differences between the observed and the calculated intensities are shown by the blue solid line.

The refined XRD patterns reveal unambiguously, for the $PrFe_{11}Ti$ and $YFe_{11}Ti$ samples, a main phase of about 98 % indexed in the tetragonal $I4/mmm$ $ThMn_{12}$-type phase. Around 2% of additional lines are assigned to bcc α-Fe.

The representative refinement results are listed in Table II. XRD patterns are indexed on the bases of tetragonal cell ($I4/mmm$ space group). The corresponding refined unit cell parameters are $a = 8.5032(3)$ Å $c = 4.7891(4)$ Å and $a = 8.5942(2)$ Å $c = 4.7893(2)$ Å for $YFe_{11}Ti$ and $PrFe_{11}Ti$, respectively. These results are in agreement with the previous studies of $YFe_{11}Ti$ [94, 125] and $PrFe_{11}Ti$ [97, 99]

In order to determine which of the three inequivalent Wyckoff sites is the most favorable for titanium atoms, the XRD pattern were refined three times, once for each site. For $PrFe_{11}Ti$, we obtained the following Bragg factors R_B equal to 5.18, 11.6 and 12.7 for titanium at sites $8i$, $8j$ and $8f$, respectively. Similar results were obtained for $YFe_{11}Ti$.

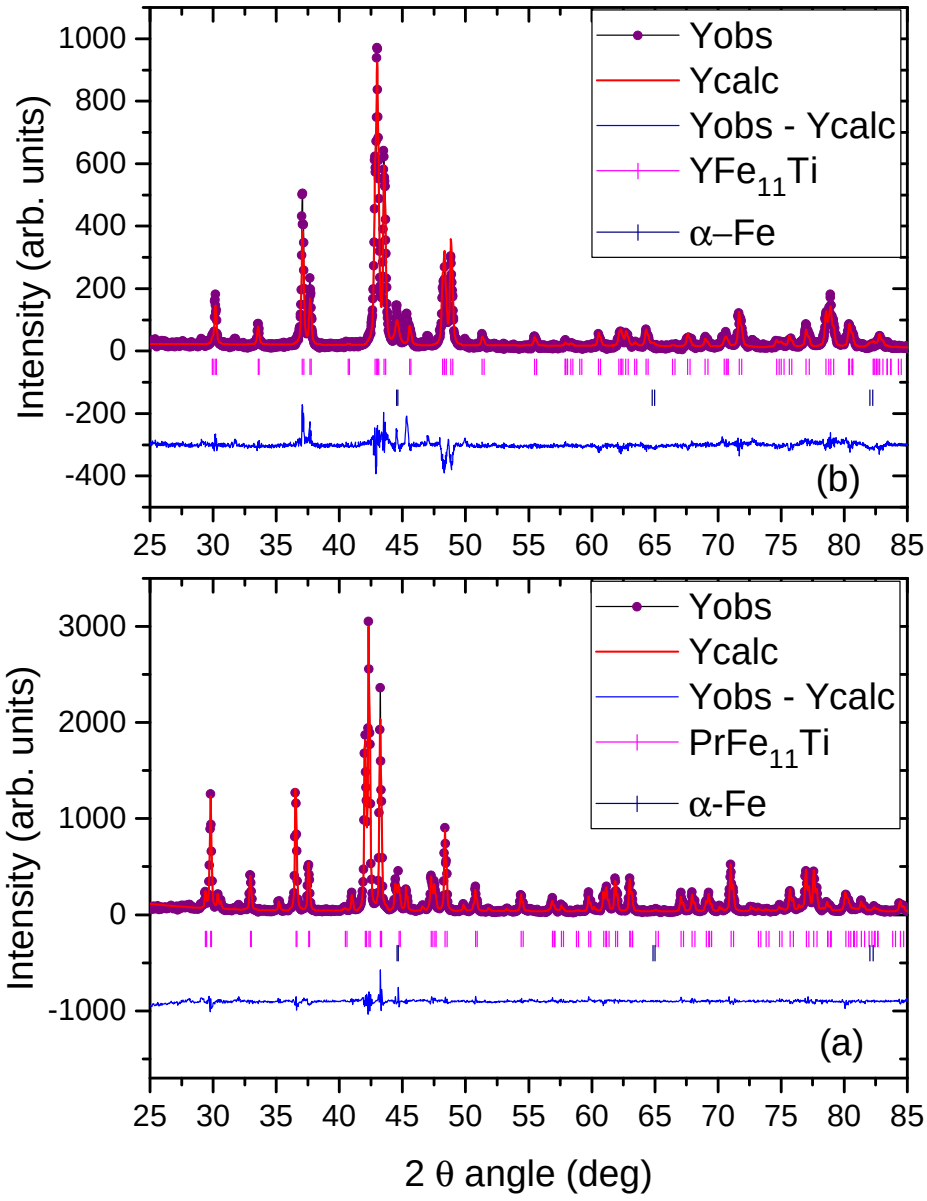

Figure 2. Rietveld refinement of XRD patterns of: (a) $PrFe_{11}Ti$, (b) $YFe_{11}Ti$. The set of ticks refers to the tetragonal $RFe_{11}Ti$ (R = Pr, Y) and α-Fe.

The best Rietveld fit corresponds to Ti atoms being located in the 8*i* sites. This result is corroborated by Mössbauer spectra analysis and the DFT calculations, that will be presented later.

Table II. a and c unit cell parameters, R_B, χ^2 factors, and atomic positions from Rietveld refinement of $RFe_{11}Ti$. (R = Y, Pr)

	$YFe_{11}Ti$	$PrFe_{11}Ti$
a (Å)	8.5032(3)	8.5942(2)
c (Å)	4.7891(4)	4.7893(2)
c/a	0.5632	0.5573
V (Å^3)	346.3	353.7
χ^2	4.73	2.68
R_B	5.37	5.18
$x\{8i\}$	0.365(2)	0.363(3)
$x\{8j\}$	0.269(2)	0.273(3)

B. Hyperfine parameters

The $ThMn_{12}$-type phase Mössbauer spectra of $YFe_{11}Ti$ and $PrFe_{11}Ti$ at $T = 300\,K$ and $T = 10\,K$ are shown in Fig. 3 and Fig. 4, respectively. Both at room temperature and at $T = 10\,K$ the Mössbauer spectra, with a clear sextets, show unambiguously that the compounds are ferromagnetic. The existence of three inequivalent crystallographic sites and the existence of Fe-Fe dumbbells ($8j$ site) connected to the Pr vacancies are responsible for the complexity of the spectra.

The three hyperfine interactions arise from the electron density at the core – the isomer shift δ, the electric field gradient –the nuclear quadrupole separation 2ε, and the unpaired electron density at the core – the hyperfine magnetic field H_{HF} [127, 128]. These three hyperfine parameters define each of the obtained ferromagnetic sextets.

Table III. Wigner-Seitz cell volume (Å^3) for $RFe_{11}Ti$.

R	$R\{2a\}$	$Fe\{8i\}$	$Fe\{8j\}$	$Fe\{8f\}$
Y	29.3	12.8	11.6	11.1
Pr	23.3	13.1	11.6	10.6

The obtained Mössbauer spectra result from the superposition of numerous ferromagnetic

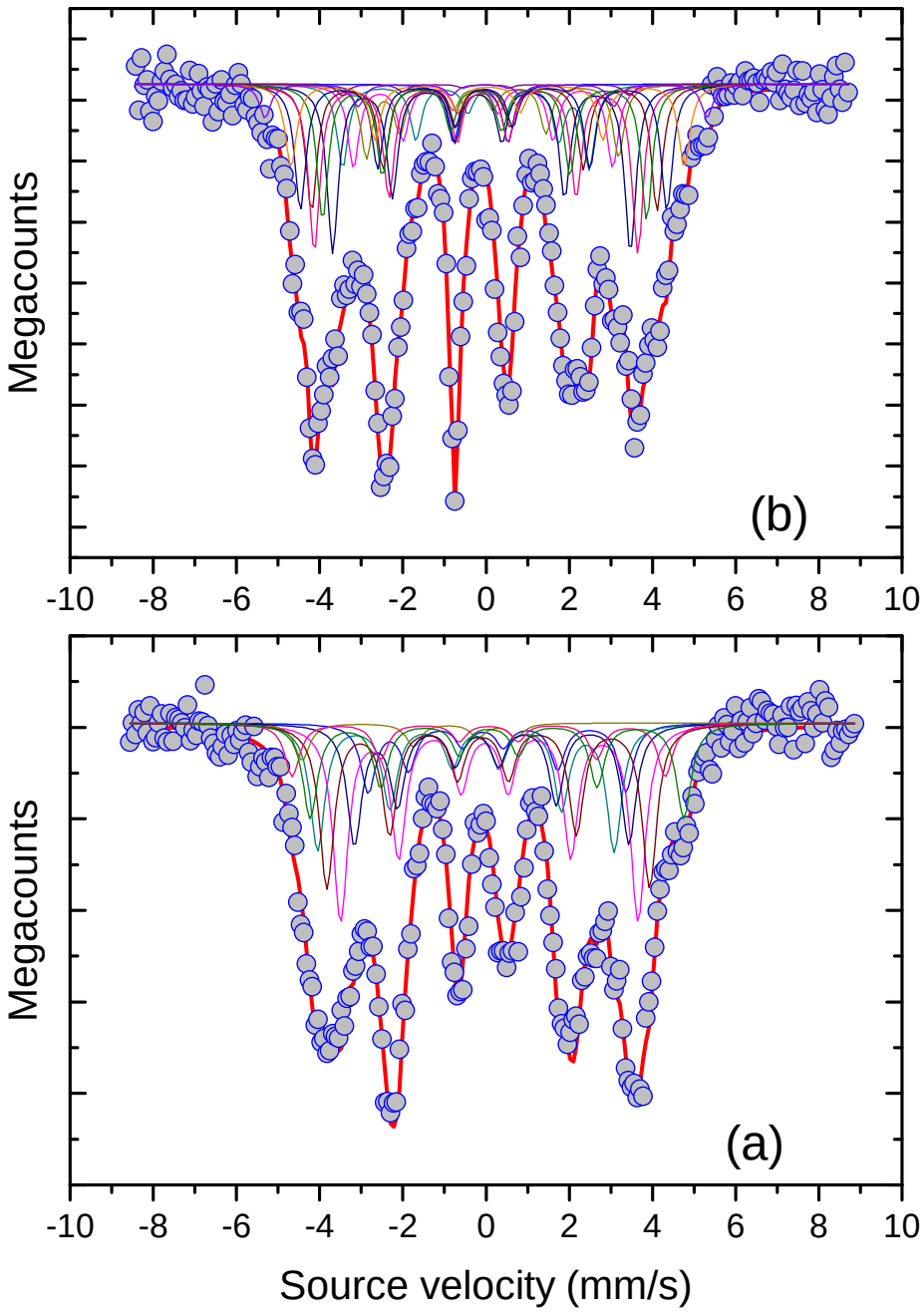

Figure 3. (a) Mössbauer spectra of $YFe_{11}Ti$ at $T = 300\,K$, (b) and at $T = 10\,K$. The red solid line and the blue circle symbol scatter plot are the calculated and experimental spectra, respectively. The color solid lines are the nine sextets used in the fit.

sextets. The different hyperfine parameters could be obtained from the refinement of these spectra. The solution must be coherent with a physical model supported by other techniques or justified by theoretical considerations. The Mössbauer analysis derives from the following two criteria:

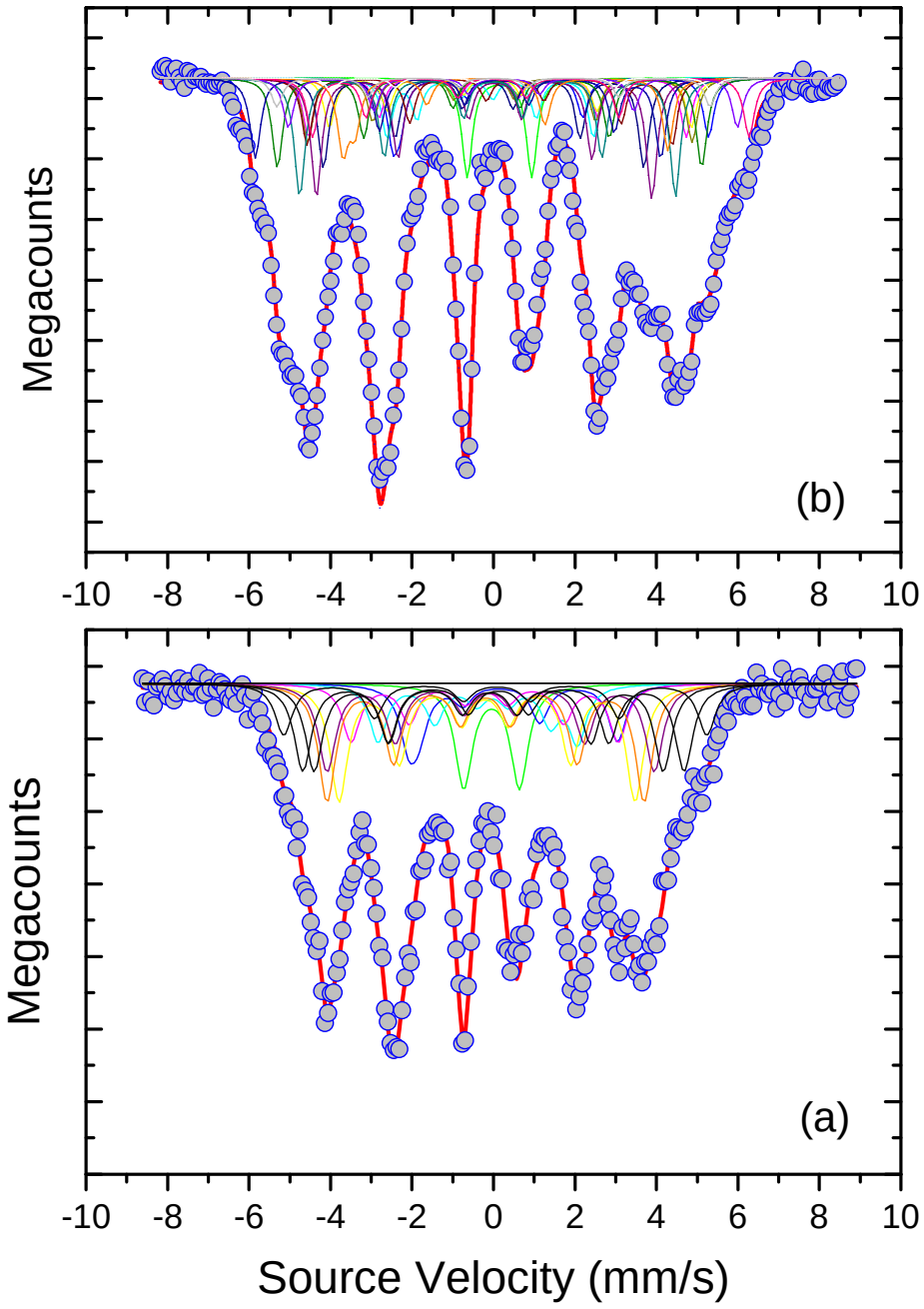

Figure 4. (a) Mössbauer spectra of $PrFe_{11}Ti$ at $T = 300\,K$ (b) and at $T = 10\,K$. The red solid line and the blue circle symbol scatter plot are the calculated and experimental spectra, respectively. The color solid lines are the nine sextets used in the fit.

- The assignment of the hyperfine parameter set to a given sextet obeys the relationship between the Wigner-Seitz cell (WSC) volumes and the isomer shift δ: the larger the WSC volume, the larger the isomer shift [97, 99, 114, 123, 129, 130].

- Given the probable substitution of Fe by Ti at site $8i/8j/8f$, in the $ThMn_{12}$ structure, the sextet abundance of the three inequivalent iron $8i$, $8j$, and $8f$ sub-sites is calculated by a multinomial distribution law.

  Let P_0 be the relative proportion of iron in the β site and P_k the relative proportion of the substitution element in the same site:

$$\sum_{k=0}^{K} P_k = 1$$

  When the atoms are randomly distributed on a site β, for a given configuration $\beta = (n_1, \ldots, n_k)$ with k varying according to the number of neighbors in the site β ($K = 4$ for $8i$ site, $K = 2$ for $8j$ site and $K = 4$ for $8f$ site), the probability P_β can be expressed as a multinomial law:

$$P_\beta = \frac{N!}{n_1! \ldots n_K!} p_1^{n_1} \times \ldots \times p_K^{n_K} \quad (1)$$

  Where, P_β is the probability of finding k Ti atoms in a shell of n $8i/8j/8f$ nearest neighbors, p_k is the relative atomic proportion of Ti atoms in different $8i/8j/8f$ sites and $N =$ is equal to 4, 2 and 4 for respectively $8i$, $8j$ and $8f$. The subspectra with intensity lower than two percent were neglected.

Using the refined crystallographic parameters (Table II), the WSC volumes were calculated by means of Dirichlet domains and coordination polyhedra for each inequivalent crystallographic site [131]. The atomic radius of Fe, Ti, Pr and Y are 1.26, 1.47, 1.82 and 1.80 Å, respectively [132]. The calculated WSC volumes are reported in Table III. The WSC volume sequence is $8i > 8j > 8f$, which is in agreement with the sequence found in RFe$_{11}$Ti series [97, 99]. This sequence of WSC volumes could explain the fact that Ti atoms, with a larger radius than iron, have a preference for the $8i$ site. This result is in agreement with the previous study using Mössbauer spectrometry [96] of SmFe$_{11}$Ti.

In addition to b.c.c α-Fe sextet, nine sextets were necessary to refine the Mössbauer spectra of YFe$_{11}$Ti and PrFe$_{11}$Ti compounds. Those sextets are due to the random occupation of the $8i$ sites by Ti atoms which induces a distribution of near-neighbor environments for the three inequivalent, $8i$, $8j$, and $8f$ crystallographic Fe sites. Having in mind that this distribution is multinomial, each $8i$, $8j$, and $8f$ sites contribute with three sextets, therefore, at least nine sextets are required to correctly fit the experimental Mössbauer spectra.

Table IV. Mössbauer hyperfine parameters for RFe$_{11}$Ti: Hyperfine field ($H_{\rm HF}$), isomer shift (δ) and quadrupole interaction (2ε). $\langle$HF$\rangle$ denotes the average of the hyperfine parameters

	R	T(K)	Fe$\{8i\}$	Fe$\{8j\}$	Fe$\{8f\}$	$\langle$HF$\rangle$
$\mu_0 H_{\rm HF}$(T)	Y	300	26.8	22.7	20.1	23.2
		10	30.9	27.6	24.3	27.6
	Pr	300	27.1	23.8	21.8	24.2
		10	31.2	28.7	26.3	28.5
δ (mm/s)	Y	300	-0.09	-0.12	-0.17	-0.13
		10	0.02	0.01	-0.02	0.01
	Pr	300	-0.08	-0.10	-0.12	-0.09
		10	0.08	0.01	-0.01	0.03
2ε (mm/s)	Y	300	0.08	0.07	0.04	0.06
		10	0.10	0.09	0.05	0.08
	Pr	300	0.09	0.09	0.04	0.08
		10	0.13	0.11	0.06	0.10

The assignment of the different sextets was done based upon the two criteria cited above, the relationship between the WSC volumes and the isomer shift, and the count of the different Fe neighboring and calculated sextet areas using a multinomial distribution. A WSC analysis of the three inequivalent iron sites in PrFe$_{11}$Ti and YFe$_{11}$Ti indicates that the $8i$ site has at 11.75 the greatest number of Fe near neighbors, while the $8j$ and $8f$ Fe sites have only 9 Fe near neighbors. Therefore, the sextets with the largest hyperfine field were assigned to the $8i$ site, based on its relative contribution and its Fe near-neighbor environment. The $8j$ and $8f$ sextets assignment was based on the isomer shift. In the fitting procedure, as the samples were random powders corroborated by XRD analysis, the line intensities of the sextet were assumed to be 3:2:1:1:2:3 in agreement with the lack of crystallographic texture. Lorentzian linewidth of 0.27 - 0.29 mm/s was used for each individual sextet. The Lamb-Mössbauer absorption factor was assumed to be the same for all crystallographic sites. All neighbor environments were considered inside a coordination sphere of 2.80 Å and we have neglected the site abundances lower than 2%. All along the

refinement process, the site abundances were maintained as fixed parameters. All other hyperfine parameters δ, $H_{\rm HF}$, and 2ε were considered as free. In the second step of the fitting, the deduced averaged isomer shift values were assigned to each site according to the WSC volume relationship. In the last step of the fit all hyperfine parameters were free.

The average hyperfine parameters has been refined and reported in Table IV. The following hyperfine field sequence $H_{\rm HF}\{8i\} > H_{\rm HF}\{8j\} > H_{\rm HF}\{8f\}$ is obtained, this result is consistent with those found for RFe$_{11}$Ti, R = Y [95, 133], Nd[99, 134], Pr [97, 99], Sm [96, 99], Gd [135], Dy, Tb, Ho and Er [99].

It is worth emphasizing that the sequence of the refined average isomer shift $\delta\{8i\} > \delta\{8j\} > \delta\{8f\}$ follows the sequence WSC volumes, in good agreement with our assumption.

In order to deduce the average magnetic moment of Fe $\langle\mu_{\rm Fe}\rangle$ from the weighted average hyperfine field $\langle H_{\rm HF}\rangle$, we can use, with a good approximation, the conversion factor of 15.6 T/$\mu_{\rm B}$ [136, 137]. For YFe$_{11}$Ti compound, we have found $\mu_0\langle H_{\rm HF}\rangle = 27.6\,$T at $T = 10\,$K, which corresponds to $\langle\mu_{\rm Fe}\rangle = 1.77\,\mu_{\rm B}$. While for PrFe$_{11}$Ti ternary compound, we have found $\mu_0\langle H_{\rm HF}\rangle = 28.5\,$T at $T = 10\,$K which corresponds to $\langle\mu_{\rm Fe}\rangle = 1.82\,\mu_{\rm B}$. These results will be compared with low temperature magnetic measurements in the next section.

C. Magnetic properties

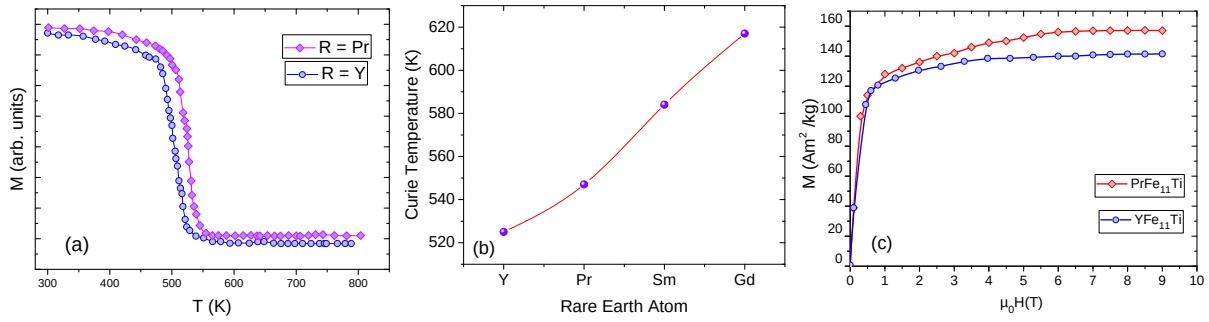

Figure 5. (a) Temperature dependence of the magnetization for RFe$_{11}$Ti measured with an appleid field of 0.1 T. (b) Curie Temperatures of some rare-earth atoms RFe$_{11}$Ti (R = Y, Pr Sm, Gd). (c) Magnetization isotherms of RFe$_{11}$Ti compounds with ThMn$_{12}$- type structure for R = Pr and R = Y measured at $T = 4.2$ K.

Fig 5 (a) shows temperature dependence of the magnetization curves of YFe$_{11}$Ti and PrFe$_{11}$Ti compounds, measured with an applied field of 0.1 T. The Curie temperatures (T_C)

Table V. Curie temperatures T_C (K), saturation magnetization M_S (Am^2/kg) at $T = 4.2$ K, magnetic moment μ_{Fe} (μ_B/atom), average magnetic moment $\langle\mu_{Fe}\rangle$ (μ_B/Fe atom) deduced from $\langle H_{HF}\rangle$, magnetic moment per transition metal μ_M (μ_B/M), the estimated anisotropy fields $\mu_0 H_A$ (T) and anisotropy constant K (MJ/m^3) for RFe$_{11}$Ti (R = Y, Pr).

R	T_C	M_S	M_S	μ_{Fe}	$\langle\mu_{Fe}\rangle$	μ_M	$\mu_0 H_A$	K
	K	Am^2/kg	μ_B/f.u.	μ_B/at.Fe	μ_B/at.Fe	μ_B/at.	T	MJ/m^3
Y	525	141	18.96	1.72	1.77	1.58	3.3	2.32
Pr	547	158	22.72	2.06	1.82	1.89	5.8	4.57

have been derived from the $M^2 - T$ curves and by extrapolating $M^2 = 0$. The values of T_C are 525 K and 547 K for YFe$_{11}$Ti and PrFe$_{11}$Ti, respectively (Table V). These results are in agreement with those reported by Piquer [97, 99], Nikitin [94] and Tereshina [95]

For a comparison some Curie temperatures for the series iron intermetallics RFe$_{11}$Ti with R = Y, Pr, Sm and Gd, are plotted in Fig 5 (b). For rare-earth transition metal intermetallic compounds, T_C is essentially controlled by Fe-Fe exchange interaction ($J_{Fe\text{-}Fe}$) which depends closely on the interatomic distances. $J_{Fe\text{-}Fe}$ ($3d-3d$) is higher than $J_{R\text{-}R}$ ($4f-4f$) and $J_{R\text{-}Fe}$ ($3d-4f$) exchange interactions [138]. As the unit cell parameters increase for RFe$_{11}$Ti series from R=Y to R=Gd [133], the interatomic distances Fe-Fe augment. Since the $J_{Fe\text{-}Fe}$ exchange interactions increase with the interatomic distances $d_{Fe\text{-}Fe}$, following the Beth-Slater curve [139], consequently, the exchange interactions increase, which contributes to the Curie temperature augmentation.

The field dependence of the magnetization for the RFe$_{11}$Ti compounds measured at T = 4.2 K are shown in Fig 5 (c). The saturation is reached slightly faster for YFe$_{11}$Ti, which can be attributed to the fact that this compound exhibits a lower magnetocrystalline anisotropy than PrFe$_{11}$Ti.

The value of the saturation magnetization was calculated using the so called "law of approach to saturation" that can be written [140, 141]:

$$M = M_S\left(1 - \frac{a}{H^2}\right) \tag{2}$$

The above equation can also be used to derive the magnetocrystalline anisotropy constant

K for the studied compounds utilizing the following relation [140, 141] :

$$K = M_S \cdot \sqrt{a \cdot \frac{105}{8}} \tag{3}$$

Consequently, from the derived anisotropy constant K and the saturation magnetization M_S, one can deduce the anisotropy field H_A with the following equation:

$$H_A = \frac{2 \cdot K}{M_S} \tag{4}$$

We have calculated M_S, $\mu_0 H_A$ and K, for the two compounds $YFe_{11}Ti$ and $PrFe_{11}Ti$, these values are reported in the Table V. We found the following values $\mu_0 H_A = 3.3\,\mathrm{T}$, $K = 2.32\,\mathrm{MJ/m^3}$, and $\mu_0 H_A = 5.8\,\mathrm{T}$, $K = 4.57\,\mathrm{MJ/m^3}$, for $YFe_{11}Ti$ and $PrFe_{11}$, respectively. These values are comparable to those found for $YFe_{11}Ti$ [94, 95, 142]. Cizmas *et al.* studied the compound $GdFe_{11}Ti$ [143], they found $\mu_0 H_A = 6.0\,\mathrm{T}$ and $K = 2.46\,\mathrm{MJ/m^3}$, the anisotropy constant is comparable to the one we found for R=Y and Pr, while the anisotropy field is higher than for our compounds.

Furthermore, we have deduced the magnetic moments of iron per formula unit μ_{Fe} from the saturation magnetizations measured at low temperature. The magnetic moments are 1.72 and 2.06 μ_{B} for $YFe_{11}Ti$ and $PrFe_{11}Ti$, respectively (Table V). These values are in very good agreement with those deduced from the weighted average hyperfine field, $\langle \mu_{\mathrm{Fe}} \rangle$, derived using the refinement of the Mössbauer spectra (Tables IV and V).

D. DFT calculations

The binary YFe_{12} is not stable and a stabilizing element such as Ti must be alloyed for obtaining the ternary $YFe_{11}Ti$ $ThMn_{12}$-type phase. In order to compare the structural stability of the hypothetical binary YFe_{12} and ternary $YFe_{11}Ti$, we evaluate the formation energy ΔE of the binary YFe_{12} and ternary $YFe_{11}Ti$ using the density functional theory. The formation energy is calculated using the following equation [144, 145]:

$$\Delta E_{\mathrm{form}} = E_{\mathrm{t}}[products] - \sum E_{\mathrm{t}}[reactants] \tag{5}$$

The estimated formation energy equations for both YFe_{12} (6) and $YFe_{11}Ti$ (7) intermetallics are defined as follows:

$$\Delta E_{\text{form}} = E_{\text{t}}[\text{YFe}_{12}] - (E_{\text{t}}[\text{Y}] + 12\, E_{\text{t}}[\text{Fe}]) \tag{6}$$

$$\Delta E_{\text{form}} = E_{\text{t}}[\text{YFe}_{11}\text{Ti}] - (E_{\text{t}}[\text{Y}] + 11\, E_{\text{t}}[\text{Fe}] + E_{\text{t}}[\text{Ti}]) \tag{7}$$

Where, E_{t} denotes the total energy of the system. The finding formation energies are $-0.9118\,\text{Ry}$ and $-0.6321\,\text{Ry}$ for YFe_{11}Ti and YFe_{12}, respectively. It is worth noting that the $\Delta E_{\text{formation}}$ of the binary system is higher than that of the ternary one, suggesting that the $I4/mmm$ structure of YFe_{11}Ti is more stable than that of the YFe_{12} tetragonal ThMn_{12} type-structure, and YFe_{12} structure can be stabilized by replacing Fe atoms by Ti atoms. This result is in agreement with the experimental analysis achieved by Buschow [146].

The total energy of YFe_{11}Ti was calculated for different sites of substitution of the iron atom by the titanium atom. We have found that the lowest energy corresponds to the substitution of one of the iron atoms at site $8i$ by the titanium atom (Table VI). This result is in agreement with that observed by neutron diffraction for $\text{YFe}_{12-x}\text{Ti}_x$ [147], these data indicate that Fe atoms preferentially occupy the $8f$ and $8j$ sites, while Ti atoms preferentially occupy the $8i$ sites. Moze and Buschow also found that the chromium atom prefers to occupy exclusively the $8i$ site for $\text{YFe}_{12-x}\text{Cr}_x$ [148].

Table VI. Calculated energy of YFe_{11}Ti with Ti atom occupying different sites.

Site	$8i$	$8j$	$8f$
E (Ry)	-36480.6233	-36480.6114	-36480.6025

The calculated spin-polarized total densities of states of $R\text{Fe}_{11}\text{Ti}$ are shown in Fig. 6 for R =Y, Pr. Fig. 7 shows a comparison of the total density of states of bcc Fe (x12) with that of the hypothetical phases YFe_{12} and PrFe_{12}. It can be seen that the DOS for YFe_{12} and PrFe_{12} corresponds mostly to the contribution of the $3d$ bands. It can also be noted that in the case of bcc Fe, for the minority spin states, the valley separating the bonding and anti-bonding orbitals is deeper and wider than in the case of YFe_{12} and PrFe_{12}. In addition, the DOS values are higher for the compound R =Pr compared to R =Y, this is due to the fact that the orbitals of the Pr atom are more populated with electrons.

Table VII. Total and local calculated magnetic moments of $R\mathrm{Fe}_{11}\mathrm{Ti}$ (R = Y, Pr)

	Total μ_{cal}	Local calculated magnetic moment				
	μ_{B}/f.u.	$R(2a)$	Fe($8i$)	Ti($8i$)	Fe($8j$)	Fe($8f$)
$\mathrm{YFe}_{11}\mathrm{Ti}$	20.04	-0.16	2.49	-0.47	2.07	1.88
$\mathrm{PrFe}_{11}\mathrm{Ti}$	23.02	1.31	2.53	-0.38	2.16	1.91

Fig. 8 shows the partial densities of states for the inequivalent crystallographic iron sites $8i$, $8j$ and $8f$ for $\mathrm{YFe}_{11}\mathrm{Ti}$ and $\mathrm{PrFe}_{11}\mathrm{Ti}$ compounds. $\mathrm{YFe}_{11}\mathrm{Ti}$ and $\mathrm{PrFe}_{11}\mathrm{Ti}$ show a relatively weak ferromagnetic state, as the spin-up bands are not completely occupied. However the local density of state of iron $8i$ sites exhibits the highest magnetic moment.

We have found that the calculated magnetic moments are 20.04 and 23.02 μ_{B} for $\mathrm{YFe}_{11}\mathrm{Ti}$ and $\mathrm{PrFe}_{11}\mathrm{Ti}$, respectively. These calculated moments are in good agreement with those deduced from the magnetization measured at low temperature (4.2 K) *i.e.* 18.96 and 22.72 μ_{B} for $\mathrm{YFe}_{11}\mathrm{Ti}$ and $\mathrm{PrFe}_{11}\mathrm{Ti}$, respectively. The results of $\mathrm{YFe}_{11}\mathrm{Ti}$ are in agreement with those calculated by Sakuma [93, 149] and Ke and Johnson [102].

The iron moment is relatively low in the tetragonal ThMn_{12} type-structure. The average iron moment, derived from th difference between the numbers of major spin and minor spin, is 1.90 μ_{B} (for $\mathrm{YFe}_{11}\mathrm{Ti}$) and 2.12 μ_{B} (for $\mathrm{PrFe}_{11}\mathrm{Ti}$), and the largest moment is 2.49 μ_{B} (for $\mathrm{YFe}_{11}\mathrm{Ti}$) and 2.53 μ_{B} (for $\mathrm{PrFe}_{11}\mathrm{Ti}$) for the $8i$ iron atom.

In Table VII we have listed the calculated local magnetic moments on the three crystallographic sites as well as the total magnetic moment per formula unit. We can see that the following magnetic moment sequence $\mu_{\mathrm{Fe}}\{8i\} > \mu_{\mathrm{Fe}}\{8j\} > \mu_{\mathrm{Fe}}\{8f\}$. This sequence follows the sequence, $H_{\mathrm{HF}}\{8i\} > H_{\mathrm{HF}}\{8j\} > H_{\mathrm{HF}}\{8f\}$, obtained for the experimental hyperfine fields fitted by Mössbauer spectrometry, and ab initio calculated hyperfine fields.

The fact that the magnetic moment of the $8f$ iron site is the smallest could be a consequence of the short Fe-Fe distances of the nearest neighbors for the $8f$ sites. One of the reasons that the iron atoms have the highest moment value at $8i$ site could be the presence of a only one nearest neighboring R atom, whereas at the other $8j$ and $8f$ sites, two R atoms are nearest neighboring.

For the compound $\mathrm{YFe}_{11}\mathrm{Ti}$, the calculation gives a small negative moment both for the Y atom - 0.16 μ_B and for the Ti atom - 0.47 μ_{B}. While for $\mathrm{PrFe}_{11}\mathrm{Ti}$, we obtained the following

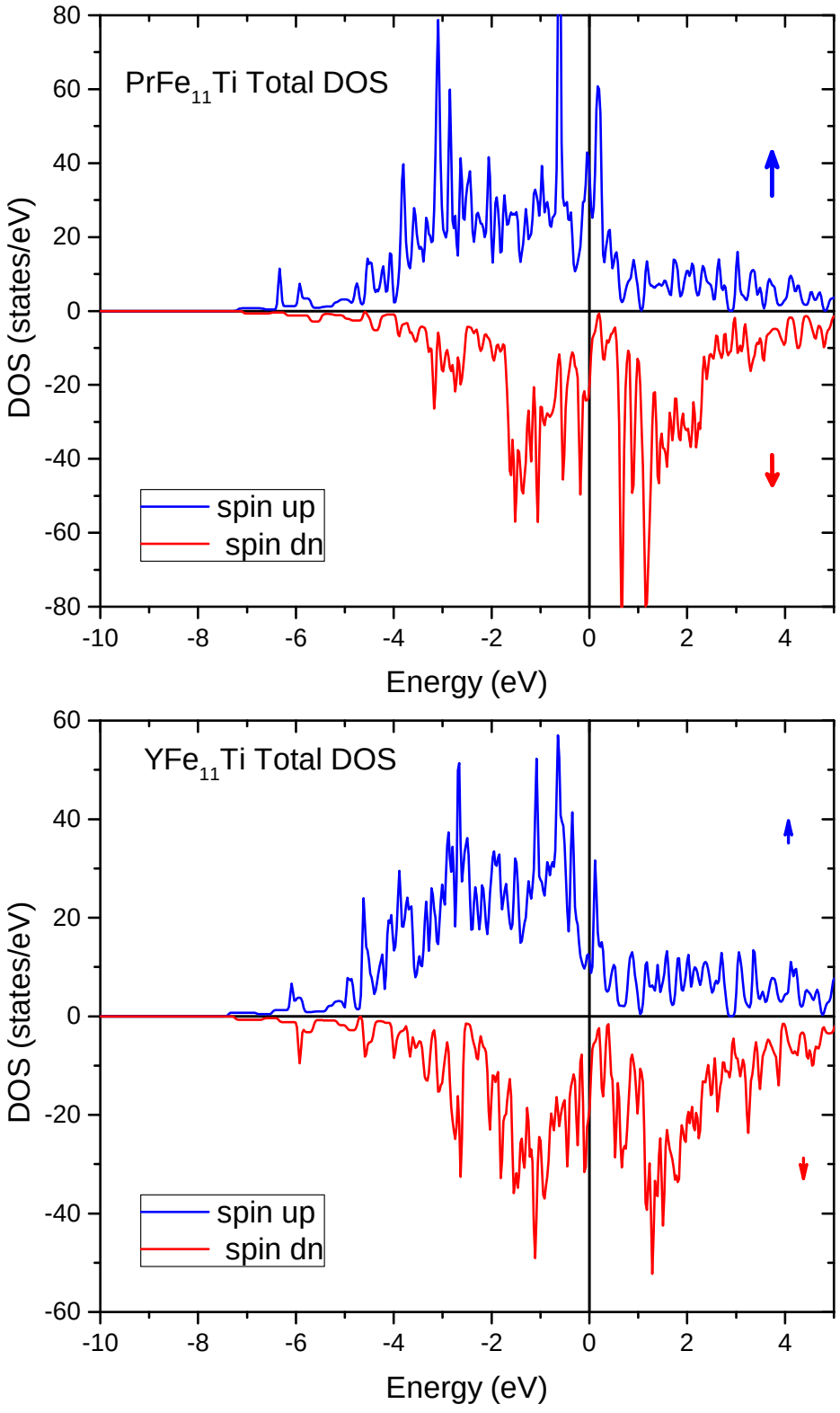

Figure 6. Total density of states of (top) $PrFe_{11}Ti$ and (down) $YFe_{11}Ti$. The origin of the energy is located at Fermi energy (black vertical line).

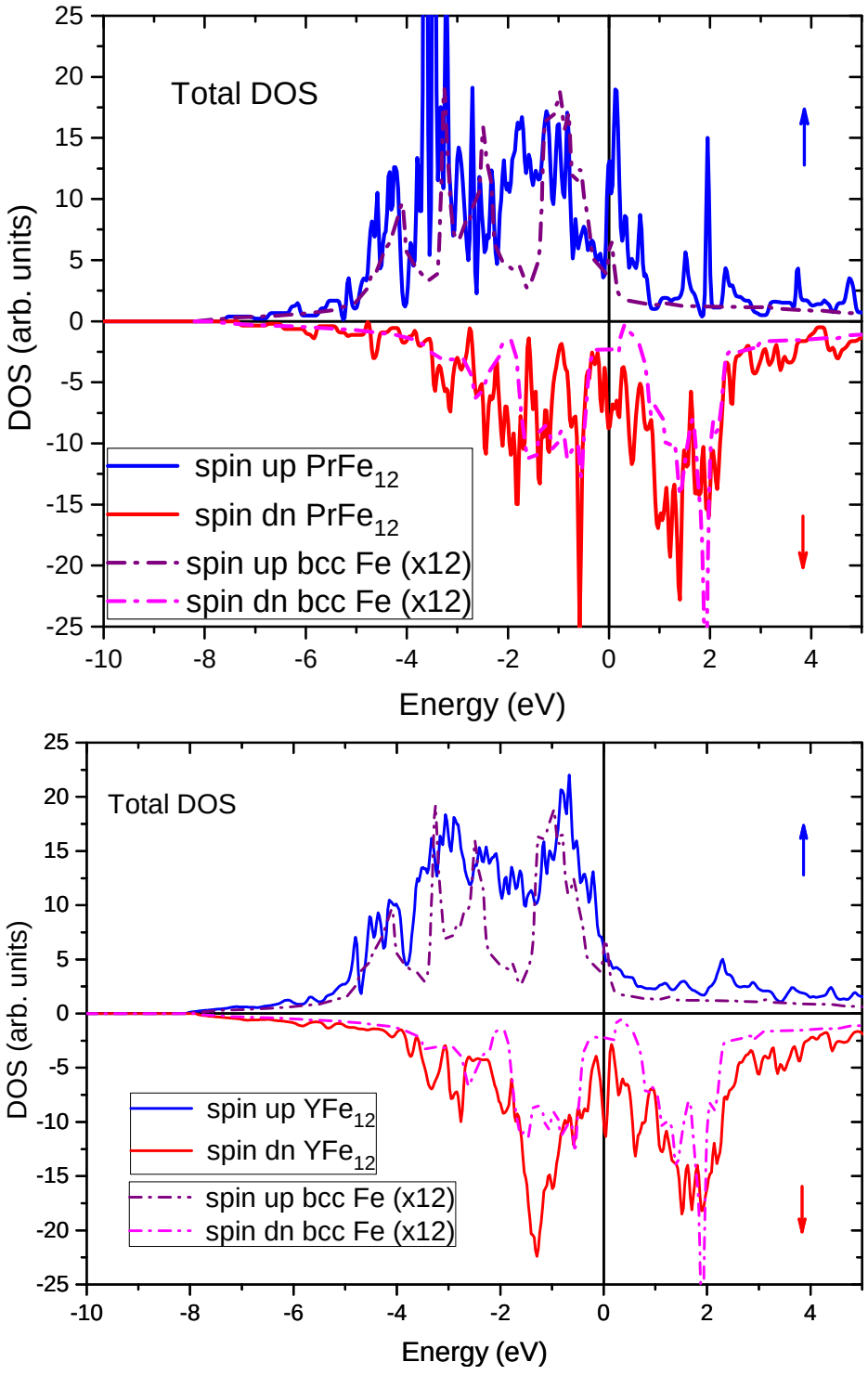

Figure 7. Total density of states of (top) $PrFe_{12}$ straight line, bcc Fe dashed line, and (down) YFe_{12} straight line, bcc Fe dashed line. The origin of the energy is located at Fermi energy (black vertical line).

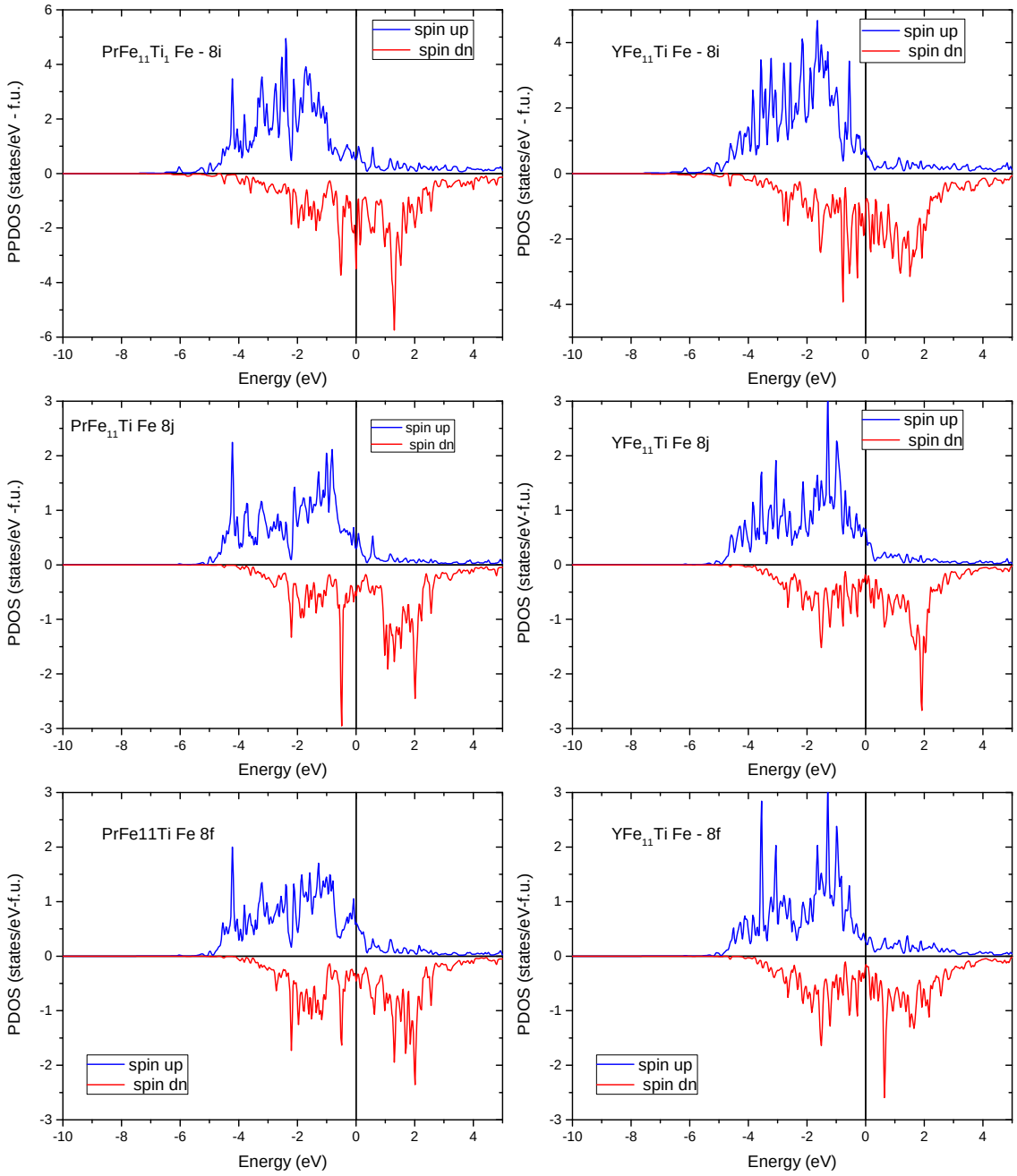

Figure 8. Partial density of states for Fe-8i, Fe 8j and Fe-8f calculated for (left) $PrFe_{11}Ti$ (right) $YFe_{11}Ti$. The origin of the energy is located at Fermi energy (black vertical line).

magnetic moments 1.31 μ_B and - 0.38 μ_B for the Pr and Ti atoms, respectively. These results are in agreement with Sakuma [93, 149] and with Ke and Johnson [102]. The negative values for the paramagnetic atoms in these intermetallics seem predictable due to the anti-parallel coupling of the atoms Y and Ti with Fe [102, 150]. This is confirmed by the partial DOS of of $PrFe_{11}Ti$ and $YFe_{11}Ti$ shown in Fig. 9. The partial DOS shows a certain overlap indicating

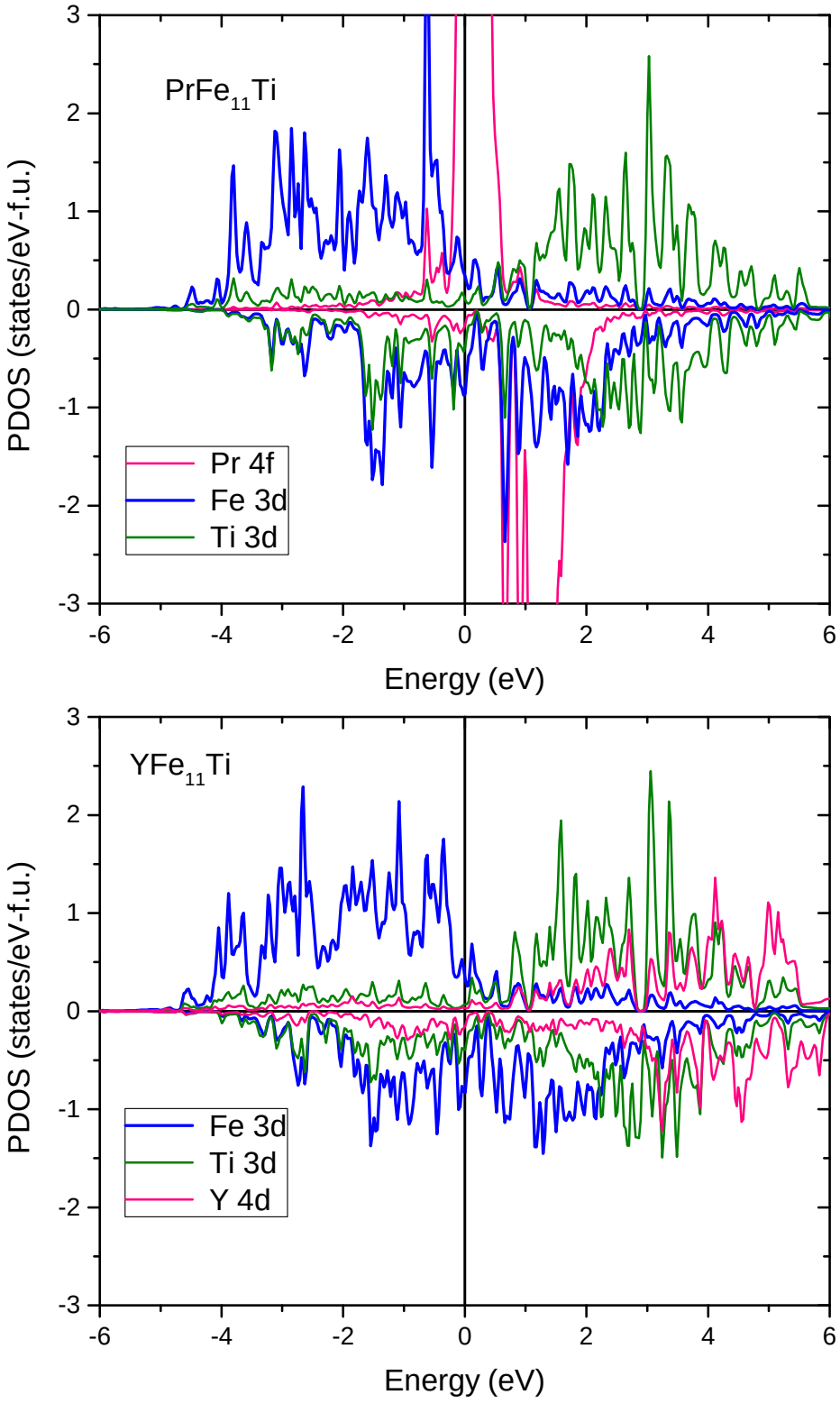

Figure 9. Partial density of states of (top) $PrFe_{11}Ti$, and (down) $YFe_{11}Ti$. The origin of the energy is located at Fermi energy (black vertical line).

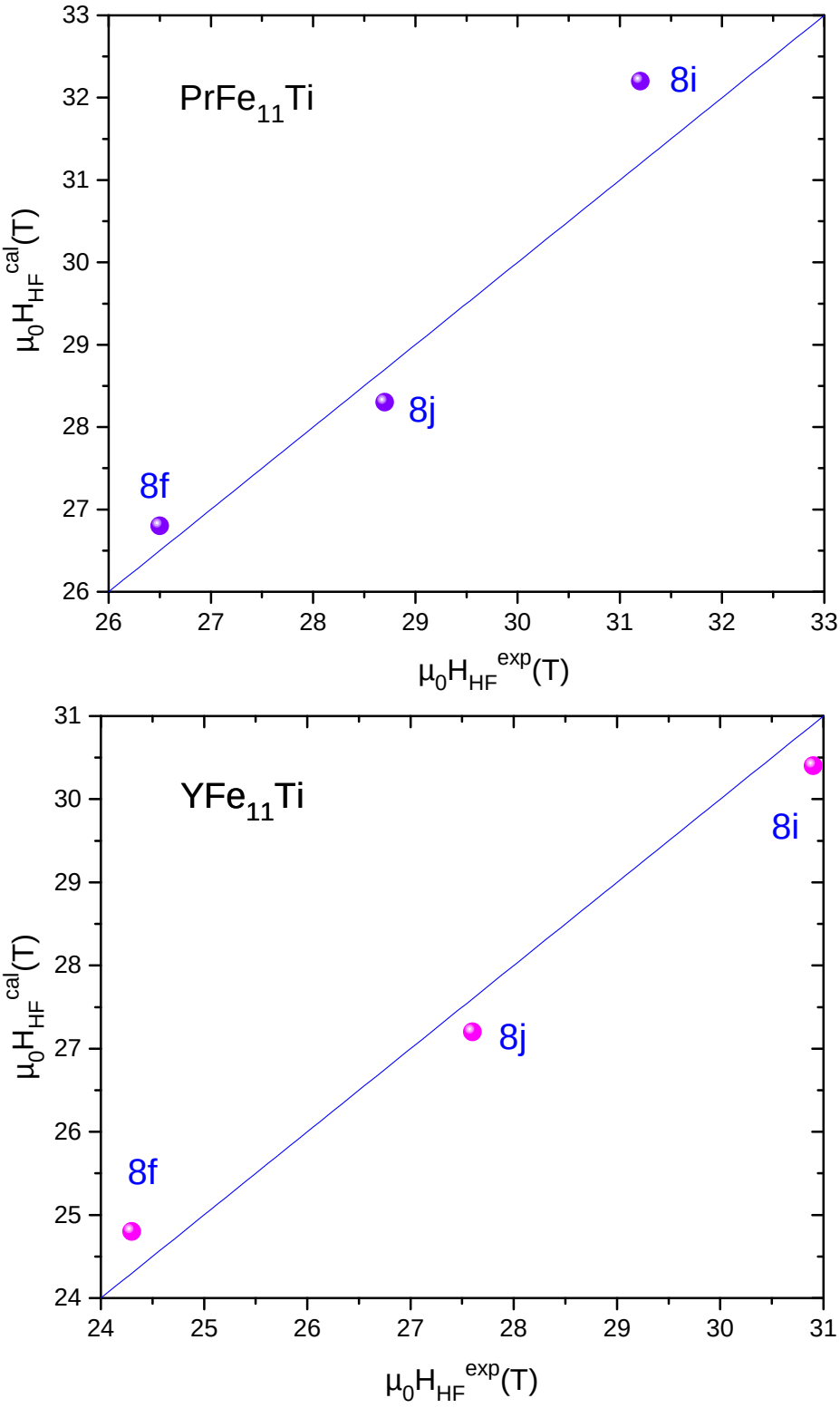

Figure 10. Calculated magnetic hyperfine field vs. the measured hyperfine field for (top) $PrFe_{11}Ti$ and (down) $YFe_{11}Ti$.

Table VIII. DFT calculated hyperfine fields (T) for RFe$_{11}$Ti

	R	8i	8j	8f
$\mu_0 H_{\rm HF}$ (T)	Y	30.4	27.2	24.8
	Pr	32.2	28.3	26.8

that the hybridization occurs for both compounds between the Ti 3d- and Fe 3d- orbitals starting from the valence band up to 2 eV of the conduction band for YFe$_{11}$Ti and up to 3 eV for PrFe$_{11}$Ti. Hybridization is more visible in the YFe$_{11}$Ti compound, it is probably for this reason that the magnetic moment of the Ti atom for PrFe$_{11}$Ti is greater than for YFe$_{11}$Ti.

Moreover, Fig. 9 shows that the 4f states of Pr are partially occupied (majority spins), while the 4f states of Pr with minority (negative) spins are empty and above the Fermi level. The DOS around E_F is rather dominated by the 3d states, mainly contributed by the Fe sub-networks. This can be understood by the fact that Pr 4f states couple anti-parallel to Fe 3d states. This result is in agreement with that found by Trygg *et al.* [151] and Liu *et al.* [152] for the GdFe$_{12}$ and Gd(Co,Fe)$_{12}$B$_6$ compounds, respectively.

In addition, we have calculated the hyperfine field for each inequivalent crystallographic iron site (table VIII). Fig. 10 shows a comparison of the calculated magnetic hyperfine magnetic vs. the experimental hyperfine fields refined from Mössbauer spectra for RFe$_{11}$Ti (R = Pr, Y) compounds. The values of these calculated hyperfine parameter are in reasonable agreement with the experimental data derived from the refinement of the Mössbauer spectra (table IV). Table IX summarize the comparison between the results of magnetic moments, obtained by experimental measurements (magnetization and Mössbauer Spectrometry) and theoretical calculations by DFT for YFe$_{11}$Ti and PrFe$_{11}$Ti. Overall, we have obtained a good agreement

V. CONCLUSION

Polycrystalline samples RFe$_{11}$Ti (R=Y, Pr) were prepared by arc-melting technique. Both compounds were investigated by XRD and are single-phase with tetragonal crystal structure and $I4/mmm$ space group. The magnetic measurements show that the Curie

Table IX. Comparison between the results of magnetic moments, in μ_B/at., obtained by experimental measurements (magnetization and Mössbauer Spectrometry) and theoretical calculations by DFT for $YFe_{11}Ti$ and $PrFe_{11}Ti$.

	Mössbauer	Magnetization	Calculated
$YFe_{11}Ti$			
$\langle\mu_{Fe}\rangle$	1.77	1.72	1.90
$\mu_{Fe}\{8i\}$	1.98	—	2.49
$\mu_{Fe}\{8j\}$	1.77	—	2.07
$\mu_{Fe}\{8f\}$	1.56	—	1.88
μ_Y	—	—	-0.16
μ_{Ti}	—	—	-0.47
$PrFe_{11}Ti$			
$\langle\mu_{Fe}\rangle$	1.82	2.06	2.12
$\mu_{Fe}\{8i\}$	2.00	—	2.53
$\mu_{Fe}\{8j\}$	1.84	—	2.16
$\mu_{Fe}\{8f\}$	1.69	—	1.91
μ_{Pr}	—	—	1.31
μ_{Ti}	—	—	-0.38

temperature T_C of $YFe_{11}Ti$ compound is lower than that of $PrFe_{11}Ti$ due to its smaller Fe-Fe exchange interaction $J_{Fe\text{-}Fe}$ compared to (R=Pr), which is confirmed by the deduced lattice parameter attesting the large crystallographic constant of R=Pr in regard for R=Y. Mössbauer spectrometry analysis provides the hyperfine parameters for the 3 inequivalent crystallographic sites $8i$, $8j$ and $8f$. We demonstrated that the titanium atoms prefer to occupy the $8i$ site by means of XRD, DFT and Mössbauer spectrometry. It was found that the calculated hyperfine field H_{HF} was in line with the experimental iron magnetic moment deduced from magnetization data. *Ab initio* calculations based on the formalism of DFT are in good agreement with the experimental data of Mössbauer and magnetization. The asymmetrical nature of density of states indicates the magnetic behavior for all compounds. The obtained total energy calculations of $YFe_{11}Ti$ shows that the lowest energy corresponds

to the substitution of the iron atoms at site $8i$ by the titanium atom, indicating that the Fe atoms preferentially occupy the $8j$ and $8f$ sites, while Ti atoms preferentially occupy the $8i$ sites. Finally, these results are helpful to understand in detail the magnetism and electronic structure in $R\mathrm{Fe}_{11}\mathrm{Ti}$ (R=Y, Pr) intermetallics. Both theoretical ab initio and experimental approaches have demonstrated to be complementary in studying magnetic properties of intemetallic R-T compounds.

ACKNOWLEDGMENTS

This work was supported by the National Center for Scientific Research (CNRS), France, and by the "Ministère de l'Éducation Nationale, de la Formation professionnelle, de l'Enseignement Supérieur et de la Recherche Scientifique", Morocco.

---

[1] G. Hadjipanaysis, S. C. Cornelison, J. A. Gerber, and D. J. Sellmyer. *J. Magn. Magn. Mater.*, 21:101–107, 1980.

[2] D. B. de Mooij and K. H. J. Buschow. *J. Less-Common. Met.*, 136:207, 1988.

[3] R. Coehoorn. *Phys. Rev. B*, 41:11790–11797, 1990.

[4] R. Coehoorn. *J. Magn. Magn. Mater.*, 99:55–70, 1991.

[5] N. H. Duc, T. D. Hien, P. E. Brommer, and J. J. M. Franse. *J. Magn. Magn. Mater.*, 104-107:1252–1256, 1992.

[6] R. Reisser, M. Seeger, and H. Kronmüller. *J. Magn. Magn. Mater.*, 128:321–340, 1993.

[7] X. C. Kou, H. Kronmuller, D. Givord, and M. F. Rossignol. *Phys. Rev. B*, 50:3849–3860, 1994.

[8] C. Djega-Mariadassou, L. Bessais, A. Nandra, and E. Burzo. *Phys. Rev. B*, 68:24406, 2003.

[9] L. Bessais, C. Djega-Mariadassou, A. Nandra, M. D. Appay, and E. Burzo. *Phys. Rev. B*, 69:64402, 2004.

[10] S. Suzuki, T. Kuno, K. Urushibata, K. Kobayashi, N. Sakuma, K. Washio, M. Yano, A. Kato, and A. Manabe. *J. Magn. Magn. Mater.*, 401:259–268, 2016.

[11] Y. Hirayama, Y.K. Takahashi, S. Hirosawa, and K. Hono. *Scr. Mater.*, 138:62–65, 2017.

[12] Y. Harashima, T. Fukazawa, and T. Miyak. *Scr. Mater.*, 179:12–15, 2020.

[13] H. M. Sanchez, D. Salazar, L. E. Zamora, J. S. T. Hernandez, J. A. Tabares, and G. A. P. Alcazar. *Hyperfine Interact.*, 241:44, 2020.

[14] D. Ogawa, T. Yoshioka, X.D. Xu, Y.K. Takahashi, H. Tsuchiura, T. Ohkubo, S. Hirosawa, and K. Hono. *J. Magn. Magn. Mater.*, 497:165965, 2020.

[15] K. H. J. Buschow. *J. Appl. Phys.*, 63:3130–3135, 1988.

[16] J. M. D Coey and H. Sun. *J. Magn. Magn. Mater.*, 87:L251–L254, 1990.

[17] A. Sakuma. *J. Appl. Phys.*, 73:6922–6924, 1993.

[18] S. A. Nikitin, I. S. Tereshina, V. N. Verbetski , and A. A. Salamova. *Phys. Solid State*, 40:258–262, 1998.

[19] I. S. Tereshina, P Gaczynski, V S Rusakov, H Drulis, S A Nikitin, W Suski, N V Tristan, and T Palewski. *J. Phys.: Condens. Matter*, 13:8161–8170, 2001.

[20] L. Bessais and C. Djega-Mariadassou. *Phys. Rev. B*, 63:054412, 2001.

[21] C. Piquer, F. Grandjean, O Isnard, V. Pop, and G. J. Long. *J. Alloys Compd.*, 377:1–7, 2004.

[22] L. Bessais, E. Dorolti, and C. Djega-Mariadassou. *Appl. Phys. Lett.*, 87, 2005.

[23] C. Piquer, F. Grandjean, O Isnard, and G. J. Long. *J. Phys.: Condens. Matter*, 18:221–242, 2006.

[24] R. Fersi, N. Mliki, L. Bessais, R. Guetari, V. Russie, and M. Cabie. *J. Alloys Compd.*, 522:14–18, 2012.

[25] S. Khazzan, L. Bessais, G. Van Tendeloo, and N. Mliki. *J. Magn. Magn. Mater.*, 363:125–132, 2014.

[26] L. Ke and D. D. Johnson. *Phys. Rev. B*, 94:024423, 2016.

[27] A. M. Schönhöbel, R. Madugundo, A.M. Gabay, J.M. Barandiaran, and G.C. Hadjipanayis. *J. Alloys Compd.*, 2019.

[28] A. Margarian, J. B. Dunlop, R. K. Day, and W. Kalceff. *J. Appl. Phys.*, 76:6153–6155, 1994.

[29] Z. Liu, Z. Jin, and C. Xia. *Scripta Mater.*, 37:1129–1134, 1997.

[30] P. Qian, N. X. Chen, , and J. Shen. *Modelling Simul. Mater. Sci. Eng.*, 13:851–860, 2005.

[31] W. Kohn and L. J. Sham. *Phys. Rev.* , 140:A1133, 1965.

[32] P. Hohenberg and W. Kohn. *Phys. Rev.* , 136:B864, 1964.

[33] P. Blaha, K. Schwarz, G. K. H. Madsen, D. Kvasnicka, J. Luitz, R. Laskowski, F. Tran, and L. D. Marks. *WIEN2k, An Augmented Plane Wave + Local Orbitals Program for Calculating*

Crystal Properties. Karlheinz Schwarz, Techn. Universität Wien, Austria, 2018, ISBN: 3-9501031-1-2.

[34] P. Blaha, K. Schwarz, F. Tran, R. Laskowski, G. K. H. Madsen, and L. D. Marks. *J. Chem. Phys.*, 152:074101, 2020.

[35] J. P. Perdew, K. Burke, and M. Ernzerhof. *Phys. Rev. Lett.*, 77:3865, 1996.

[36] K. Schwarz and P. Blaha. *Comput. Mater. Sci.*, 28:259, 2003.

[37] S. Blügel, H. Akai, R. Zeller, and P. H. Dederichs. *Phys. Rev. B*, 35:3271–3283, 987.

[38] S Khazzan, N Mliki, L Bessais, and C Djega-Mariadassou. *J. Magn. Magn. Mater.*, 322(2):224–229, 2010.

[39] R. Bensalem, W. Tebib, S. Alleg, J. J. Sunol, L. Bessais, and J. M. Greneche. *J. Alloys Compd.*, 471:24–27, 2009.

[40] A. Hamrita, Y. Slimani, M. K. Ben Salem, E. Hannachi, L. Bessais, F. Ben Azzouz, and M. Ben Salem. *Ceram. int.*, 40:1461–1470, 2014.

[41] J. Rodríguez-Carvajal. *Physica B* , 192:55, 1993.

[42] J. Rodríguez-Carvajal, M. T. Fernandez-Diaz, and J. L. Martinez. *J. Phys.* , 81:210, 2000.

[43] H. Rietveld. *Acta Crystallogr.*, 22:151, 1967.

[44] H. Rietveld. *J. Appl. Crystallogr.*, 2:65, 1969.

[45] L. Bessais, S. Sab, C. Djega-Mariadassou, N. H. Dan, and N. X. Phuc. *Phys. Rev. B*, 70:134401, 2004.

[46] K. Younsi, V. Russier, and L. Bessais. *J. Appl. Phys.*, 107:083916, 2010.

[47] S. Khazzan, N. Mliki, and L. Bessais. *J. Appl. Phys.*, 105:103904, 2009.

[48] K. H. J. Buschow. *Rep. Prog. Phy.*, 40:1179, 1977.

[49] B. P. Hu, H. S. Li, and J. M. D. Coey. *J. Appl. Phys.*, 67:4838–4840, 1990.

[50] Z. Hu, W. B. Yelon, S. Mishra, Gary J. Long, O. A. Pringle, D. P. Middleton, K. H. J. Buschow, and F. Grandjean. *J. Appl. Phys.*, 67:4838–4840, 1994.

[51] Brent Fultz. *Characterization of Materials*, chapter Mössbauer Spectrometry. John Wiley, New York, 2011.

[52] N. Bouchaala, M. Jemmali, T. Bartoli, K. Nouri, I. Hentech, S. Walha, L. Bessais, and A. Ben Salah. *journal of solid state chemistry*, 258:501–209, 2018.

[53] E. Burzo. *Rep. Prog. Phys.* , 61:1099, 1998.

[54] M. Forker, A. Julius, M. Schulte, and D. Best. *Phys. Rev. B*, 57:11565, 1998.

[55] L. Bessais, C. Djega-Mariadassou, and E. Koch. *J. Phys.: Condens. Matter*, 14:8111, 2002.

[56] E. T. Teatum, K. A. Gschneidner, and J. T. Waber. *Rep. LA-4003.* Los Alamos Scientific Lab, Los Alamos, NM, 1968.

[57] Z W Li, X Z Zhou, and A H Morrish. *J. Phys.: Condens. Matter*, 4:10409–10420, 1992.

[58] C. Piquer, F. Grandjean, O Isnard, V. Pop, and G. J. Long. *J. Appl. Phys.*, 95:6308, 2004.

[59] C Piquer, O Isnard, F Grandjean, and G J Long. *J. Magn. Magn. Mater.*, 263:235–242, 2003.

[60] B. P. Hu, H. S. Li, J. P. Gavigan, and J. M. D. Coey. *J. Phys.: Condens. Matter*, 1:755–770, 1989.

[61] C. J. M. Denissen, R. Coehoorn, and K. H. J. Buschow. *J. Magn. Magn. Mater.*, 87:51–56, 1990.

[62] E. du Trémolet de Lacheisserie (et al.). *Magnetism - Materials and Applications.* Speinger-Verlag New York, 2005.

[63] Z. W. Li and X. A. H. Morrish. *Phys. Rev. B*, 55:3670–3676, 1997.

[64] L. Néel. *J. Phys. Radium*, 9:148, 1948.

[65] B. Cullity. *Introduction to Magnetic Materials.* Addison-Wesley Publishing Company, 1972.

[66] Q. N. Qi, Y. P. Li, and J. M. D. Coey. *J. Phys.: Condens. Matter*, 4:8209–8220, 1992.

[67] C. B. Cizmas, C. Djega-Mariadassou, and L. Bessais. *J. Alloys Compd.*, 345:27–35, 2002.

[68] M. Bhihi, M. Lakhal, H. Labrim, A. Benyoussef, A. El Kenz, O. Mounkachi, and E. K. Hlil. *Chin. Phys. B*, 21:097501, 2012.

[69] Y. Harashima, T. Fukazawa, H. Kino, and T. Miyake. *J. Appl. Phys.*, 124:163902, 2018.

[70] K. H. J. Buschow. *J. Appl. Phys.*, 63:3130, 1988.

[71] Y. Yang, X. Zhang, L. Kong, and Q. Pan. *Solid State Comm.* , 78:313–316, 1991.

[72] O. Moze and K. H. J. Buschow. *J. Alloys Compd.*, 233:165–168, 1996.

[73] A. Sakuma. *J. Phys. Soc. Jpn.*, 61:4119–4124, 1993.

[74] J. G. M. Armitage, T. Dumelow, P. C. Riedi, and J. S. Abell. *J. Phys.: Condens. Matter*, 1:3987–3994, 1989.

[75] J. Trygg, B. Johansson, and M. S. S. Brooks. *J. Magn. Magn. Mater.*, 104-107:1447–1448, 1992.

[76] X. B. Liu, Z. Altounian, and D. H. Ryan. *J. Alloys Compd.*, 688:118–122, 2016.

[77] G. Hadjipanaysis, S. C. Cornelison, J. A. Gerber, and D. J. Sellmyer. *J. Magn. Magn. Mater.*, 21:101–107, 1980.

[78] D. B. de Mooij and K. H. J. Buschow. *J. Less-Common. Met.*, 136:207, 1988.

[79] R. Coehoorn. *Phys. Rev. B*, 41:11790–11797, 1990.

[80] R. Coehoorn. *J. Magn. Magn. Mater.*, 99:55–70, 1991.

[81] N. H. Duc, T. D. Hien, P. E. Brommer, and J. J. M. Franse. *J. Magn. Magn. Mater.*, 104-107:1252–1256, 1992.

[82] R. Reisser, M. Seeger, and H. Kronmüller. *J. Magn. Magn. Mater.*, 128:321–340, 1993.

[83] X. C. Kou, H. Kronmuller, D. Givord, and M. F. Rossignol. *Phys. Rev. B*, 50:3849–3860, 1994.

[84] C. Djega-Mariadassou, L. Bessais, A. Nandra, and E. Burzo. *Phys. Rev. B*, 68:24406, 2003.

[85] L. Bessais, C. Djega-Mariadassou, A. Nandra, M. D. Appay, and E. Burzo. *Phys. Rev. B*, 69:64402, 2004.

[86] S. Suzuki, T. Kuno, K. Urushibata, K. Kobayashi, N. Sakuma, K. Washio, M. Yano, A. Kato, and A. Manabe. *J. Magn. Magn. Mater.*, 401:259–268, 2016.

[87] Y. Hirayama, Y.K. Takahashi, S. Hirosawa, and K. Hono. *Scr. Mater.*, 138:62–65, 2017.

[88] Y. Harashima, T. Fukazawa, and T. Miyak. *Scr. Mater.*, 179:12–15, 2020.

[89] H. M. Sanchez, D. Salazar, L. E. Zamora, J. S. T. Hernandez, J. A. Tabares, and G. A. P. Alcazar. *Hyperfine Interact.*, 241:44, 2020.

[90] D. Ogawa, T. Yoshioka, X.D. Xu, Y.K. Takahashi, H. Tsuchiura, T. Ohkubo, S. Hirosawa, and K. Hono. *J. Magn. Magn. Mater.*, 497:165965, 2020.

[91] K. H. J. Buschow. *J. Appl. Phys.*, 63:3130–3135, 1988.

[92] J. M. D Coey and H. Sun. *J. Magn. Magn. Mater.*, 87:L251–L254, 1990.

[93] A. Sakuma. *J. Appl. Phys.*, 73:6922–6924, 1993.

[94] S. A. Nikitin, I. S. Tereshina, V. N. Verbetski , and A. A. Salamova. *Phys. Solid State*, 40:258–262, 1998.

[95] I. S. Tereshina, P Gaczynski, V S Rusakov, H Drulis, S A Nikitin, W Suski, N V Tristan, and T Palewski. *J. Phys.: Condens. Matter*, 13:8161–8170, 2001.

[96] L. Bessais and C. Djega-Mariadassou. *Phys. Rev. B*, 63:054412, 2001.

[97] C. Piquer, F. Grandjean, O Isnard, V. Pop, and G. J. Long. *J. Alloys Compd.*, 377:1–7, 2004.

[98] L. Bessais, E. Dorolti, and C. Djega-Mariadassou. *Appl. Phys. Lett.*, 87, 2005.

[99] C. Piquer, F. Grandjean, O Isnard, and G. J. Long. *J. Phys.: Condens. Matter*, 18:221–242, 2006.

[100] R. Fersi, N. Mliki, L. Bessais, R. Guetari, V. Russie, and M. Cabie. *J. Alloys Compd.*, 522:14–18, 2012.

[101] S. Khazzan, L. Bessais, G. Van Tendeloo, and N. Mliki. *J. Magn. Magn. Mater.*, 363:125–132, 2014.

[102] L. Ke and D. D. Johnson. *Phys. Rev. B*, 94:024423, 2016.

[103] A. M. Schönhöbel, R. Madugundo, A.M. Gabay, J.M. Barandiaran, and G.C. Hadjipanayis. *J. Alloys Compd.*, 2019.

[104] A. Margarian, J. B. Dunlop, R. K. Day, and W. Kalceff. *J. Appl. Phys.*, 76:6153–6155, 1994.

[105] Z. Liu, Z. Jin, and C. Xia. *Scripta Mater.*, 37:1129–1134, 1997.

[106] P. Qian, N. X. Chen, , and J. Shen. *Modelling Simul. Mater. Sci. Eng.*, 13:851–860, 2005.

[107] W. Kohn and L. J. Sham. *Phys. Rev.* , 140:A1133, 1965.

[108] P. Hohenberg and W. Kohn. *Phys. Rev.* , 136:B864, 1964.

[109] P. Blaha, K. Schwarz, G. K. H. Madsen, D. Kvasnicka, J. Luitz, R. Laskowski, F. Tran, and L. D. Marks. *WIEN2k, An Augmented Plane Wave + Local Orbitals Program for Calculating Crystal Properties*. Karlheinz Schwarz, Techn. Universität Wien, Austria, 2018, ISBN: 3-9501031-1-2.

[110] P. Blaha, K. Schwarz, F. Tran, R. Laskowski, G. K. H. Madsen, and L. D. Marks. *J. Chem. Phys.*, 152:074101, 2020.

[111] J. P. Perdew, K. Burke, and M. Ernzerhof. *Phys. Rev. Lett.*, 77:3865, 1996.

[112] K. Schwarz and P. Blaha. *Comput. Mater. Sci.*, 28:259, 2003.

[113] S. Blügel, H. Akai, R. Zeller, and P. H. Dederichs. *Phys. Rev. B*, 35:3271–3283, 987.

[114] S Khazzan, N Mliki, L Bessais, and C Djega-Mariadassou. *J. Magn. Magn. Mater.*, 322(2):224–229, 2010.

[115] R. Bensalem, W. Tebib, S. Alleg, J. J. Sunol, L. Bessais, and J. M. Greneche. *J. Alloys Compd.*, 471:24–27, 2009.

[116] A. Hamrita, Y. Slimani, M. K. Ben Salem, E. Hannachi, L. Bessais, F. Ben Azzouz, and M. Ben Salem. *Ceram. int.*, 40:1461–1470, 2014.

[117] J. Rodríguez-Carvajal. *Physica B* , 192:55, 1993.

[118] J. Rodríguez-Carvajal, M. T. Fernandez-Diaz, and J. L. Martinez. *J. Phys.* , 81:210, 2000.

[119] H. Rietveld. *Acta Crystallogr.*, 22:151, 1967.

[120] H. Rietveld. *J. Appl. Crystallogr.*, 2:65, 1969.

[121] L. Bessais, S. Sab, C. Djega-Mariadassou, N. H. Dan, and N. X. Phuc. *Phys. Rev. B*, 70:134401, 2004.

[122] K. Younsi, V. Russier, and L. Bessais. *J. Appl. Phys.*, 107:083916, 2010.

[123] S. Khazzan, N. Mliki, and L. Bessais. *J. Appl. Phys.*, 105:103904, 2009.

[124] K. H. J. Buschow. *Rep. Prog. Phy.*, 40:1179, 1977.

[125] B. P. Hu, H. S. Li, and J. M. D. Coey. *J. Appl. Phys.*, 67:4838–4840, 1990.

[126] Z. Hu, W. B. Yelon, S. Mishra, Gary J. Long, O. A. Pringle, D. P. Middleton, K. H. J. Buschow, and F. Grandjean. *J. Appl. Phys.*, 67:4838–4840, 1994.

[127] Brent Fultz. *Characterization of Materials*, chapter Mössbauer Spectrometry. John Wiley, New York, 2011.

[128] N. Bouchaala, M. Jemmali, T. Bartoli, K. Nouri, I. Hentech, S. Walha, L. Bessais, and A. Ben Salah. *journal of solid state chemistry*, 258:501–209, 2018.

[129] E. Burzo. *Rep. Prog. Phys.* , 61:1099, 1998.

[130] M. Forker, A. Julius, M. Schulte, and D. Best. *Phys. Rev. B*, 57:11565, 1998.

[131] L. Bessais, C. Djega-Mariadassou, and E. Koch. *J. Phys.: Condens. Matter*, 14:8111, 2002.

[132] E. T. Teatum, K. A. Gschneidner, and J. T. Waber. *Rep. LA-4003.* Los Alamos Scientific Lab, Los Alamos, NM, 1968.

[133] Z W Li, X Z Zhou, and A H Morrish. *J. Phys.: Condens. Matter*, 4:10409–10420, 1992.

[134] C. Piquer, F. Grandjean, O Isnard, V. Pop, and G. J. Long. *J. Appl. Phys.*, 95:6308, 2004.

[135] C Piquer, O Isnard, F Grandjean, and G J Long. *J. Magn. Magn. Mater.*, 263:235–242, 2003.

[136] B. P. Hu, H. S. Li, J. P. Gavigan, and J. M. D. Coey. *J. Phys.: Condens. Matter*, 1:755–770, 1989.

[137] C. J. M. Denissen, R. Coehoorn, and K. H. J. Buschow. *J. Magn. Magn. Mater.*, 87:51–56, 1990.

[138] E. du Trémolet de Lacheisserie (et al.). *Magnetism - Materials and Applications.* Speinger-Verlag New York, 2005.

[139] Z. W. Li and X. A. H. Morrish. *Phys. Rev. B*, 55:3670–3676, 1997.

[140] L. Néel. *J. Phys. Radium*, 9:148, 1948.

[141] B. Cullity. *Introduction to Magnetic Materials*. Addison-Wesley Publishing Company, 1972.

[142] Q. N. Qi, Y. P. Li, and J. M. D. Coey. *J. Phys.: Condens. Matter*, 4:8209–8220, 1992.

[143] C. B. Cizmas, C. Djega-Mariadassou, and L. Bessais. *J. Alloys Compd.*, 345:27–35, 2002.

[144] M. Bhihi, M. Lakhal, H. Labrim, A. Benyoussef, A. El Kenz, O. Mounkachi, and E. K. Hlil. *Chin. Phys. B*, 21:097501, 2012.

[145] Y. Harashima, T. Fukazawa, H. Kino, and T. Miyake. *J. Appl. Phys.*, 124:163902, 2018.

[146] K. H. J. Buschow. *J. Appl. Phys.*, 63:3130, 1988.

[147] Y. Yang, X. Zhang, L. Kong, and Q. Pan. *Solid State Comm.* , 78:313–316, 1991.

[148] O. Moze and K. H. J. Buschow. *J. Alloys Compd.*, 233:165–168, 1996.

[149] A. Sakuma. *J. Phys. Soc. Jpn.*, 61:4119–4124, 1993.

[150] J. G. M. Armitage, T. Dumelow, P. C. Riedi, and J. S. Abell. *J. Phys.: Condens. Matter*, 1:3987–3994, 1989.

[151] J. Trygg, B. Johansson, and M. S. S. Brooks. *J. Magn. Magn. Mater.*, 104-107:1447–1448, 1992.

[152] X. B. Liu, Z. Altounian, and D. H. Ryan. *J. Alloys Compd.*, 688:118–122, 2016.